Amorphous Pullulan Trehalose Microparticle Platform for Respiratory Delivery

*Nicholas B. Carrigy, Mani Ordoubadi, Yushan Liu, Omar Melhem, David Barona, Hui Wang, Leanne Milburn, Conor A. Ruzycki, Warren H. Finlay, Reinhard Vehring**

Department of Mechanical Engineering, University of Alberta, Edmonton, Canada

Running Header: Spray Dried Pullulan Trehalose Platform

*Corresponding Author

Prof. Reinhard Vehring

University of Alberta, Department of Mechanical Engineering

10-203 Donadeo Innovation Centre for Engineering

9211 116th Street NW, Edmonton, Alberta, T6G 1H9, Canada

Telephone: +1 780 492 5180

E-mail: reinhard.vehring@ualberta.ca

Abstract

Spray drying biologics and small-molecule drugs can increase their thermal stability relative to liquid dosage forms and allow for widespread distribution to developing countries without cold chain infrastructure. In this study, pullulan trehalose powder is spray dried for inhalation. The powder is characterized in terms of manufacturability, physical stability, device compatibility, and aerosol performance. The manufacturability is demonstrated by reasonable spray drying yield and powder flowability. The powder has relatively low cohesiveness and high compressibility without semi-elastic deformation. Short-term

physical stability for ambient temperature dry storage and 40°C storage in commercial pressurized metered-dose inhaler propellants HFA 134a and HFA 227 is shown. A theoretical model predicts a high glass transition temperature near the surface of the microparticles where biologics are expected to reside. Emission from a commercial dry powder inhaler demonstrates high dispersibility, optimal size for inhalation, and adequate total lung dose, exceeding many commercial inhalation devices. The powder can be filled, stored, and actuated from a pressurized metered-dose inhaler without changes in particle morphology or solid phase. The pullulan trehalose platform thus appears promising for respiratory delivery.

Keywords: biologics, droplet chain, particle engineering, radial glass transition temperature, Raman spectroscopy, spray drying

Abbreviations: FPF = fine particle fraction; GSD = geometric standard deviation; HFA = hydrofluoroalkane; MMAD = mass median aerodynamic diameter; MOC = micro-orifice collector

1 Introduction

Biologics and small-molecule drugs are not always stable as a liquid dosage form at room temperature, and developing countries with endemic infectious diseases do not always have access to cold-chain infrastructure (Carrigy & Vehring, 2019); therefore, methods to increase thermal stability are of interest. One such method is spray drying, which consists of atomizing a liquid formulation into droplets in a hot drying gas that evaporates the solvent, leaving the solute to form solid microparticles that are collected. In addition to increased thermal stability due to decreased water-mediated degradation, solid dosage forms have less weight and volume due to solvent removal, which minimizes transportation costs and storage space requirements (Walters et al., 2014). Additionally, dry powder delivery with inhalers removes the contamination risks and disposal issues associated with needles. As compared to lyophilization, spray drying is relatively low cost and a much faster process for producing dry powder (Schwartzbach, 2011; Siew, 2016). Furthermore, particle size and properties are controlled in a single step in spray drying, making secondary milling unnecessary.

Biologics are gaining pharmaceutical market share relative to small molecules (Evaluate Ltd., 2017). Biologics are used as prophylactic agents, e.g. vaccines, against infectious diseases, and as therapeutic agents against cancers, arthritis, diabetes, and other conditions (Walsh, 2014). Examples of biologics that have been stabilized by spray drying include monoclonal antibodies, recombinant human DNase, insulin, antigens, interleukin, bacteriophage, antimicrobial peptides, bacterial cell wall hydrolases, and various vaccines (Carrigy & Vehring, 2019). The most commonly researched excipient combination for spray drying biologics is leucine and trehalose (Carrigy & Vehring, 2019). The leucine is typically designed

to be crystalline in order to increase surface roughness and thus aid dispersibility from dry powder inhalers, while trehalose solidifies to a glassy solid that protects the biologic against desiccation. However, leucine can crystallize under typical spray drying conditions and therefore be incapable of providing glass stabilization. Pullulan does not crystallize under typical spray drying conditions and therefore may be useful as an alternative excipient to leucine for stabilizing biologics. Previous work has demonstrated that pullulan and trehalose combinations stabilize β-Galactosidase in lyophilized powder (Teekamp et al., 2017), various proteins in air-dried and freeze-dried orodispersible films (Tian et al., 2018), and bacteriophages in air-dried films (Leung et al., 2018). Further characterization and understanding of pullulan trehalose microparticles is therefore of interest.

Pullulan $(C_6H_5O_{10})_n$ is a linear exopolysaccharide produced by microorganisms that forms a slimy layer around the cell wall to protect against desiccation (di Stefano, 2017). Pullulan is commonly used in industry as a film-forming agent (Leathers, 2003) and is "generally recognized as safe" in the food industry (European Food Safety Authority, 2004; United States Food and Drug Administration, 2019a), being non-toxic and non-carcinogenic (Rekha & Sharma, 2007). Industrial production techniques are reviewed elsewhere (Sugumaran & Ponnusami, 2017). Pullulan is a non-reducing sugar and is relatively impermeable to oxygen (Rekha & Sharma, 2007). It has a high glass transition temperature (Teekamp et al., 2017), ~261°C. Teekamp *et al.* (2017) showed that pullulan prevented trehalose from crystallizing at high humidity and temperature, thus improving physical stability.

Trehalose, $C_{12}H_{22}O_{11}$, is a non-reducing disaccharide also produced by microorganisms to protect against desiccation (Crowe et al., 1998). Trehalose is "generally recognized as safe" for use in foods (United States Food and Drug Administration, 2019b). It is a commonly used

excipient for stabilizing biologics (Ohtake & Wang, 2011). Trehalose has been suggested to be an excellent glass stabilizer because it has a high glass transition temperature, high hydration number, and small size (Carrigy & Vehring, 2019).

The feasibility of pullulan trehalose powder as a formulation platform for inhalation products has not previously been assessed. In this paper, pullulan trehalose powder, produced either with a monodisperse droplet chain or a spray dryer, is characterized in terms of particle formation, morphology, glass stabilizing properties, manufacturability, powder packing properties, aerosol performance, and delivery device compatibility.

2 Materials and Methods

2.1 Monodisperse Droplet Chain

2.1.1 Experimental Procedure

Particle morphology was examined using a monodisperse droplet chain described elsewhere (Gomez et al., 2018), to gain insight into the particle formation mechanism. Briefly, feed solutions of pullulan (Product no. J66961; Alfa Aesar, Tewksbury, MA, USA) and trehalose (Cat. No. BP2687; Fisher BioReagents, NH, USA) with a fixed total initial solute concentration of 1.875 mg/mL were formulated with the following excipient content combinations by percent mass of pullulan/trehalose: 0/100, 5/95, 10/90, 20/80, 40/60, 70/30, and 100/0. Heated gas at an initial temperature of 70°C entered a drying cylinder in a laminar flow at a rate of 5 L/min to evaporate the solvent and generate monodisperse dry microparticles. Individual droplets of the feed solutions were dispensed and injected into the cylinder at a frequency of 60 Hz using a piezoelectric droplet dispenser (MicroFab Technologies, Plano, TX, USA) with a 40 µm diameter micro-jet orifice. Images of the droplets were acquired

immediately after the exit of the dispenser using a high-magnification camera with a collimated light source to determine the initial droplet diameters, according to a method described previously (Gomez et al., 2018).

2.1.2 Normalized Volume Equivalent Diameter - Experiment

The volume equivalent diameter of the collected dry microparticles produced by the monodisperse droplet chain was determined experimentally for comparison to theoretical predictions from particle formation models. The dried particles that exited the droplet chain cylinder were collected at ambient conditions using a collection stub. The particles on the stub were then imaged with a field emission scanning electron microscope (Zeiss Sigma FESEM, Oberkochen, Germany). The scanning electron microscope settings were a 3.00 kV accelerating voltage, 5000x magnification, 6-7 mm working distance, and use of an immersion lens (in-lens) detector. A gold coating of ~16 nm was applied prior to imaging with a sputter deposition system (Denton II; Denton Vacuum LLC, Moorestown, NJ, USA). The Feret diameter based on the longest dimension, which represents the hydrodynamic, or volume equivalent, diameter was determined using image analysis (ImageJ, National Institutes of Health, Bethesda, MD, USA). The volume equivalent diameter of the dry microparticles was normalized by the initial droplet diameter, as the initial droplet diameter varied slightly between experiments.

2.1.3 Normalized Volume Equivalent Diameter – Analytical Particle Formation Model

An analytical particle formation model was developed with the purpose of providing a method for quickly calculating volume equivalent diameter of the dry microparticles with reasonable accuracy, without the need for numerical methods. The analytical particle

formation model (cf. the appendix for details) for multi-component systems was used to calculate the time until amorphous co-solidification occurs on the surface of a droplet, $t_{\mathrm{t,mix}}$,

$$t_{\mathrm{t,mix}} = \tau_{\mathrm{D}} \left[1 - \left(\sum_{\mathrm{i}} E_{\mathrm{i}} P_{\mathrm{i}} \right)^{\frac{2}{3}} \right] \quad (1)$$

where τ_{D} is the droplet lifetime, E_{i} is the surface enrichment of component i, and P_{i} is a non-dimensional number relating the initial solute concentration of component i to its true density.

The droplet lifetime is given by (Vehring, 2008)

$$\tau_{\mathrm{D}} = \frac{d_0^2}{\kappa} \quad (2)$$

where κ is the evaporation rate taken as 4.0×10^{-9} m^2/s (Vehring et al., 2007).

The surface enrichment of component i is approximated by (Vehring et al., 2007)

$$E_{\mathrm{i}} = 1 + \frac{Pe_{\mathrm{i}}}{5} + \frac{Pe_{\mathrm{i}}^2}{100} - \frac{Pe_{\mathrm{i}}^3}{4000} \quad (3)$$

where the Péclet number of component i is given by (Vehring et al., 2007)

$$Pe_{\mathrm{i}} = \frac{\kappa}{8 D_{\mathrm{i}}} \quad (4)$$

where D_{i} is the diffusion coefficient of solute i in the droplet solvent. The diffusion coefficient of trehalose in water was taken as 5.0×10^{-10} m^2/s (Vehring et al., 2007). The diffusion coefficient of pullulan in water was taken as 2.8×10^{-11} m^2/s, which corresponds to a molecular mass of 115 kDa (Nishinari et al., 1991).

The non-dimensional number P_{i} is defined as (Vehring, 2008)

$$P_{\mathrm{i}} = \frac{C_{0,\mathrm{i}}}{\rho_{\mathrm{t,i}}} \quad (5)$$

where $C_{0,\mathrm{i}}$ is the initial solute concentration of component i and $\rho_{\mathrm{t,i}}$ is the true density of component i. The true densities of trehalose and pullulan were assumed to be 1580 kg/m^3 (Grasmeijer et al., 2016) and 1850 kg/m^3 (Sangon Biotech, 2018), respectively.

The d^2 law, which assumes a constant evaporation rate and hence constant temperature, was used to estimate the volume equivalent diameter at the time of co-solidification at the surface

$$d_{\mathrm{v}}^2 = d_0^2 - \kappa t_{\mathrm{t,mix}} \quad (6)$$

where the experimentally determined initial droplet diameter, explained in Section 2.1.2, was used for calculation. The volume equivalent diameter of the dry microparticles were normalized by the initial droplet diameter as per Section 2.1.2.

2.1.4 Normalized Volume Equivalent Diameter - Numerical Particle Formation Model with Viscosity Correction

A numerical particle formation model similar to one described previously (Ordoubadi et al., 2018) was used to predict the volume equivalent diameter for comparison to the analytical model and experimental results. The model is based on a one-dimensional numerical solution to Fick's second law within a spherical droplet, including the effect of Stefan flow. Internal circulation was neglected. The concentration varied with radius as the dimensionless Péclet number, representing the ratio of evaporative surface recession to mass diffusivity, was on the order of 10 for pullulan. The droplet temperature was assumed to be spatially homogeneous as the dimensionless Lewis number, representing the ratio of thermal diffusivity to mass diffusivity, was on the order of 100. As Baldelli *et al.* (2016)

demonstrated, viscosity increases during drying due to increases in solute concentration as water solvent evaporates. This decreases the diffusion coefficient, increases the Péclet number, increases the surface enrichment, and leads to earlier solidification at the surface, and larger predicted diameter. These effects were incorporated into the numerical model, with viscosity modelled as a function of solute concentration using trehalose viscosity values from the literature (Ekdavi-Sever et al., 2003). The volume equivalent diameter at the time solidification starts near the surface was an output of the model. The volume equivalent diameter of the dry particles were normalized by the experimentally measured initial droplet diameter as in Sections 2.1.2 and 2.1.3.

2.1.5 Radial Profiles of Local Mass Fractions and Dry Glass Transition Temperature

The radial profile of mass fractions and glass transition temperature is useful for predicting physical and biological stabilization potential at different locations within the microparticles. Using the output for the final radial composition of mass fractions in the microparticles from the multi-component numerical model with viscosity correction described in Section 2.1.4, the radial glass transition temperature profile was predicted using the Gordon-Taylor equation (Gordon & Taylor, 1952), modified to be a function of radius, according to

$$T_{\mathrm{g,dry}}(r) = \frac{\omega_{\mathrm{T}}(r) T_{\mathrm{g,T,dry}} + k\omega_{\mathrm{P}}(r) T_{\mathrm{g,P,dry}}}{\omega_{\mathrm{T}}(r) + k\omega_{\mathrm{P}}(r)} \quad (7)$$

where $T_{\mathrm{g,dry}}(r)$ is the dry glass transition temperature of well-mixed pullulan and trehalose which varies with radius r, $\omega_{\mathrm{T}}(r)$ and $\omega_{\mathrm{P}}(r)$ are the radial mass fractions of trehalose and pullulan, respectively, from the numerical model, $T_{\mathrm{g,T,dry}}$ and $T_{\mathrm{g,P,dry}}$ were assumed to be 394 K and 534 K, respectively, and k was assumed to be 0.4163 (Teekamp et al., 2017).

2.2 Spray Drying

2.2.1 Spray Drying Process Parameters

Relative to the droplet chain technique, spray drying has a much higher dry powder production rate, allowing for further characterization with techniques requiring large powder batches. The spray drying process was designed to yield inhalable amorphous powder that is physically stable at room temperature. A modified Büchi B-191 spray dryer (Büchi Labortechnik AG; Flawil, Switzerland), described previously (Carrigy & Vehring, 2019), in combination with a twin-fluid atomizer, was used in this study. Process parameters chosen were an inlet temperature of 80°C, corresponding to an evaporation rate of 4.8×10^{-9} m^2/s (Vehring et al., 2007), a drying gas flow rate of 540 L/min, a feed flow rate (spray rate) of 0.5 mL/min, and an atomizer air-to-liquid ratio of 14, which corresponds to an initial droplet mass median diameter of around 7 µm based on droplet size data for the twin-fluid atomizer (Hoe et al., 2014). Feed solutions were formulated with a fixed total initial solute concentration of 50 mg/mL and the following excipient content combinations by percent mass of pullulan/trehalose: 0/100, 5/95, 10/90, 17/83, 20/80, 30/70, 40/60, and 100/0. The outlet temperature, outlet relative humidity, and powder moisture content were predicted to be 61°C, 0.8%, and 0.2%, respectively, using a process model given elsewhere (Carrigy & Vehring, 2019).

2.2.2 Spray Dried Particle Morphology

Particle morphology was examined using scanning electron microscopy for spray dried particles with various excipient content combinations. The same scanning electron microscopy settings described in Section 2.1.2 were used. Additionally, a gallium beam in a helium ion microscope (Zeiss Orion NanoFab Helium Ion Microscope with Gallium Focused Ion Beam, Oberkochen, Germany) was used to cut 40% pullulan 60% trehalose

microparticles and the internal structure was subsequently imaged using the same helium ion microscope.

2.2.3 Modulated Differential Scanning Calorimetry Measurements

The reversing heat flow was determined experimentally using modulated differential scanning calorimetry (Q1000, TA Instruments, New Castle, DE, USA) to elucidate if a radial distribution of glass transition temperature was present within the microparticles by comparison to theoretical models. The test conditions were equilibration at 25°C, isothermal hold for 5 minutes, and a ramp of 5°C/min up to 340°C with a modulation of ± 2°C/min. A dry nitrogen purge of 60 mL/min was used to keep the cell dry. The mass of powder was 2.2-2.6 mg for each measurement. The spray dried powder for these measurements contained either 100% pullulan at a solids content of 20 mg/mL, 100% trehalose at a solids content of 100 mg/mL, or 16.7% pullulan and 83.3% trehalose at a total solids content of 120 mg/mL. For these measurements the inlet temperature to the spray dryer was 70°C and the initial droplet diameter was predicted to be 9 µm.

The Fox equation (Fox, 1956) is a simple method for predicting the dry glass transition temperature of a mixture, $T_{\mathrm{g,dry}}$,

$$T_{\mathrm{g,dry}} = \frac{1}{\sum_{\mathrm{i}} \frac{Y_{\mathrm{i}}}{T_{\mathrm{g,i}}}} \tag{8}$$

where $T_{\mathrm{g,i}}$ represents the glass transition temperature of component i.

Another simple method for predicting the glass transition temperature is the Gordon-Taylor equation (Gordon & Taylor, 1952), previously given by equation (7), but with the use of constant mass fractions, corresponding to the initial solute mass fractions, rather than mass

fractions at the end of the drying process that vary with radius within the microparticles. The same values for the constants were used as in Section 2.1.5. The results from these two simplified models were compared to predictions using equation (7), which uses local, radial mass fractions of pullulan and trehalose within the microparticles.

2.2.4 Modulated Compressed Bulk Density Measurements

Modulated compressed bulk density measurements were performed to determine the packing properties of the powder, using an apparatus described elsewhere (Shahrbabak, 2013). Briefly, ~100 mg of the spray dried powder generated according to Section 2.2.1 was loaded into a cylindrical cavity and the force required to compress the powder to a specified volume was measured using a load cell located below the cavity. Displacement modulation was incorporated to differentiate between plastic (reversible) and semi-elastic (non-reversible) compression, the latter of which is recognized by the powder not returning to its initial volume on decompression. The relative humidity during the measurement was set to 0% using dry nitrogen purge. A transition pressure was defined as halfway between the last data point without semi-elastic deformation and the first data point with semi-elastic deformation, with typical compression increments of 40 µm. The compressed bulk density was reported at the transition pressure. Spray dried pullulan trehalose powders were tested in the range of 0-40% pullulan content.

2.2.5 Dry Powder Inhaler Aerosol Performance Measurements

To examine the aerosolization performance of the spray dried pullulan trehalose powder generated according to Section 2.2.1, emissions from a commercial low-resistance dry powder inhaler (Seebri® Breezhaler®, Novartis International AG; Basel, Switzerland) were measured downstream of an Alberta Idealized Throat (built in-house) using a Next

Generation Impactor (Copley Scientific; Nottingham, UK). A custom mouthpiece adapter was rapid-prototyped with a PolyJet 3D printer (Objet Eden 350 V High Resolution 3D Printer, Stratsys, Ltd.; Eden Prarie, MN, USA) out of an acrylic compound (Objet VeroGray RGD850; Eden Prarie, MN, USA) and connected the dry powder inhaler to the Alberta Idealized Throat.

The powder was filled into dried size 3 hydroxypropyl methylcellulose capsules (Quali-V®-I; Qualicaps, Inc., Madrid, Spain) which are specifically designed for dry powder inhalers. These capsules are similar to the capsules used in the commercial Breezhaler® dry powder inhaler. The powder was manually filled into the capsules in a dry (< 0.1% relative humidity) environment, as verified by a hygrometer (MI70 Measurement Indicator with HMP77B humidity and temperature probe; Vaisala, Vantaa, Finland). The fill mass was 42 ± 9 mg per capsule. The filled capsules were kept dry prior to use. Three dry powder inhaler actuations and inhalations were performed, using three different powder-filled capsules, in order to capture sufficient mass on the impactor plates for accurate gravimetric measurement. The process was replicated twice for spray dried pullulan/trehalose with percent masses of 0/100, 10/90, and 40/60. To mitigate bounce, the plates of the Next Generation Impactor and the interior of the Alberta Idealized Throat were coated with silicone spray (Molykote™ 316 Silicone Release Spray, Dow Corning Corporation; Midland, MI, USA) and left to evaporate for 20 minutes. A blank run, with no capsule in the dry powder inhaler, verified that this time was sufficient for complete solvent evaporation, as the mean ± standard deviation of the mass change of the plates was 0.0 ± 0.1 mg.

Dry powder inhaler actuation was carried out according to the Breezhaler® pamphlet instructions. The capsule was pierced and inserted into the dry powder inhaler, and the dry

powder inhaler then connected by the custom mouthpiece adapter to the throat and impactor. A critical flow controller (Critical Flow Controller Model TPK 2000, Copley Scientific Limited; Nottingham, UK) set a constant flow rate of 100 L/min through the system for 2.4 seconds, resulting in a 4 L inhalation volume, as recommended in the USP-601 monograph (United States Pharmacopeia, 2017). These are the conditions recommended if a 100 L/min flow rate results in a pressure drop of less than 4 kPa (United States Pharmacopeia, 2017), which was the case as the pressure drop across the dry powder inhaler and throat was measured to be 3.4 kPa at 100 L/min using a differential pressure sensor (Model HSCDRRD160MDSA3, Honeywell; Morris Plains, NJ, USA). This is a reasonable value based on data in the literature (Krüget et al., 2014; Ruzycki et al., 2018). The cut-off diameters of the impactor stages at this flow rate are 6.12 µm (stage 1), 3.42 µm (stage 2), 2.18 µm (stage 3), 1.31 µm (stage 4), 0.72 µm (stage 5), 0.40 µm (stage 6), 0.24 µm (stage 7), and 0.07 µm for the micro-orifice collector (MOC) (Marple et al., 2003).

The emitted dose was defined as the percent of the fill mass that was emitted from the dry powder inhaler, based on the weight of the dry powder inhaler before and after emission. The total lung dose was defined as the percent of the emitted dose that is collected in the impactor (Matinkhoo et al., 2011), i.e., the dose collected downstream of the Alberta Idealized Throat. The fine particle fraction (FPF) was defined as the percent of the emitted dose that was collected on the impactor stages 2-MOC, i.e., with a size < 6.12 µm. The mass median aerodynamic diameter (MMAD) and geometric standard deviation (GSD) were determined by fitting the data to a cumulative distribution function,

$$y = \frac{1}{2}\left[1 + \mathrm{erf}\left(\frac{\ln(x) - a}{b\sqrt{2}}\right)\right] \quad (9)$$

where $a = \ln(MMAD)$ and $b = \ln(GSD)$. The fit was performed using "cftool" in MATLAB (MathWorks, Inc., Natick, MA, USA). For each run the fit was performed with x as a column vector containing the upper size limits for stages 2-MOC (for example, the upper size limit is 6.12 µm for stage 2) and y as a column vector containing the corresponding cumulative mass data that ranged from 0-1. Note that the fit was performed using data from stages 2-MOC, since the pre-separator was not used and therefore no upper size limit was available for stage 1 (Ruzycki et al., 2018).

2.2.6 Pressurized Metered-Dose Inhaler Physical Stability Measurements

The 40% pullulan 60% trehalose spray dried powder generated according to Section 2.2.1 was hand-filled with a crimper-filler (Lab Plant, Pamasol AG, Pfäffikon, Switzerland) into pressurized metered-dose inhaler canisters, either glass or aluminium, at concentrations of ~1 mg/mL in propellants hydrofluoroalkane (HFA) 134a or HFA 227. After sonication, actuation of 5-10 doses through a low-flow-rate single-nozzle impactor, described previously (Wang et al., 2017), allowed for collection of dry particles on a collection stub for scanning electron microscope imaging. The canisters were stored at room temperature or at 40°C in an incubator at ambient relative humidity for 42 days and then re-sampled using the same method for both scanning electron microscopy and solid phase analysis using a Raman spectroscopy instrument developed by Wang *et al.* (2014). Solid phase analysis was also performed for the spray dried powder kept in a dry box at ambient temperature for 42 days to verify the powder retained its amorphous solid phase without use of refrigeration or insertion into propellant.

2.3 Statistics

Student's t-tests were performed without assuming equal variance at a significance level of 0.05. Experimental results are generally presented as mean ± standard deviation of replicate measurements, with the number of replicates indicated in the text.

3 Results and Discussion

3.1 Monodisperse Droplet Chain

3.1.1 Microparticle Morphology

Scanning electron microscope images of the microparticles produced by the droplet chain are given in Figure 1. The produced microparticles were evidently monodisperse, despite folding. The folding occurs to a greater extent with increasing pullulan content in the formulation and results in more irregular, non-spherical, microparticles. This is explained by the particle engineering theory that with increasing pullulan concentration, the shell formation occurs earlier in the drying process due to higher Péclet numbers for pullulan. Subsequently, for higher pullulan contents, the shell folding begins earlier in the drying process, while the particle is relatively large and the shell thin. Further investigation would be required to fully understand the folding process. It is possible that the folded morphology for higher pullulan contents is also related to the high structural flexibility of pullulan (Kato et al., 1982). Interparticle forces may also affect folding (Tsapis et al., 2005). External voids are evident in each case. More rugose particles are typically advantageous for dispersibility.

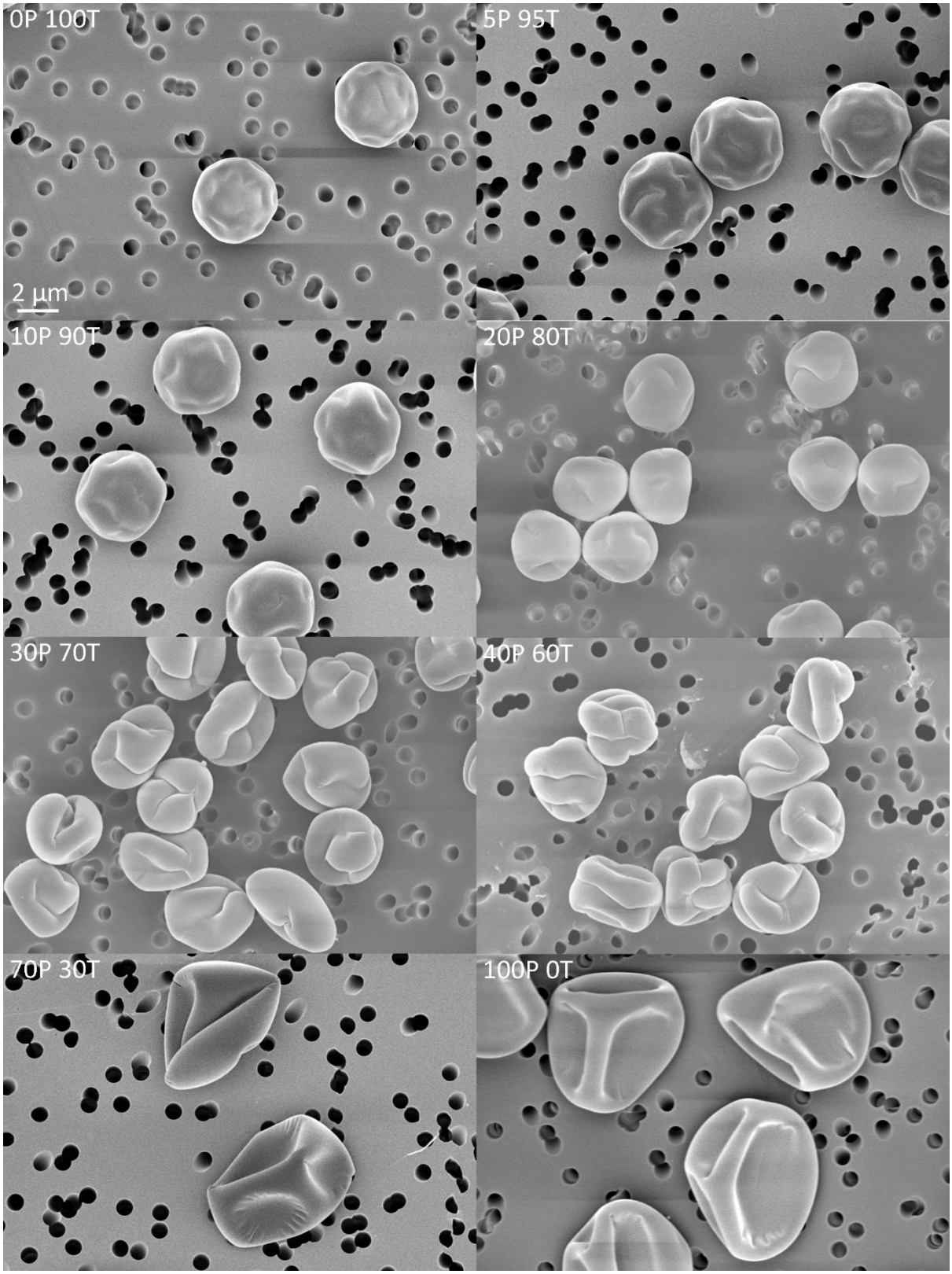

Figure 1. Scanning electron microscope images of particles produced using a monodisperse droplet chain technique. More folding is observed for particles with a higher mass fraction

of pullulan. As an example of the legend, 30P 70T represents 30% pullulan 70% trehalose powder. The same scale bar applies to all images.

3.1.2 Normalized Volume Equivalent Diameter

For the droplet chain experiments, the Péclet numbers for pullulan and trehalose were 18 and 1.0, respectively. This corresponded to respective steady state surface enrichments of 6.3 and 1.2. The range of initial droplet diameters for all (n = 15) droplet chain experiments was 29-33 μm, with an overall mean ± standard deviation of 31 ± 1 μm.

Figure 2 shows the predicted normalized volume equivalent diameters from the two models and the experimental results for comparison. The experimental values and numerical predictions matched fairly closely; an exact match was not expected as the models do not account for the shell folding or particle contraction processes. The developed particle formation models may thus give reasonable but not exact predictions for other combinations of amorphous excipients that co-solidify. The analytical model tends to under-predict the diameter as it does not account for increased surface enrichment due to increased viscosity during drying. As expected, a larger normalized diameter is predicted for the numerical model which includes viscosity effects, as this leads to higher surface enrichment and earlier predicted co-solidification. Over-prediction of diameter was observed for the numerical model, perhaps related to particle contraction after shell formation that was not modelled. Both models predict increased diameter at higher pullulan contents, as true density at the surface is predicted to be reached earlier. This trend is verified by the experimental results.

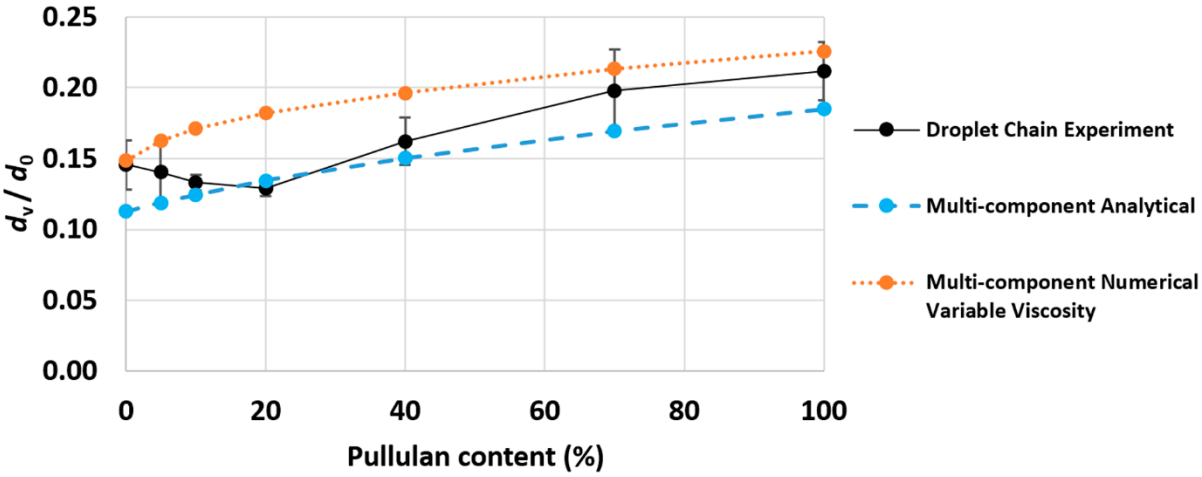

Figure 2. Experimental results and model predictions of volume equivalent diameter, d_v, normalized by initial droplet diameter, d_0, for different pullulan contents, demonstrating the reasonable accuracy of the particle formation models. Error bars represent standard deviation of two replicates, except for the 0% pullulan content case which represents three replicates. Colour version available online.

3.1.3 Radial Profiles of Local Mass Fractions and Dry Glass Transition Temperature

The numerical modelling results for the internal distributions of pullulan and trehalose mass fractions in the microparticles and the internal dry glass transition temperature radial profiles are given in Figure 3 and Figure 4, respectively. From Figure 3 it is apparent that pullulan concentrates on the surface of the microparticles even at a low overall mass fraction, and the mass fraction at the surface increases with increasing overall mass fraction of pullulan in the formulation. The high mass fraction of pullulan at the surface leads to an increase in the dry glass transition temperature near the surface, as shown in Figure 4. Since biologics are likely to reside near the surface due to their large size and low diffusion coefficient, use of pullulan is likely to increase the glass transition temperature in the vicinity of the biologic. The higher glass transition temperature near the surface may

improve biologic stabilization and may also help prevent merging between particles during temporary temperature or relative humidity excursions, thus keeping the powder dispersible. In all cases, some trehalose is present at the surface, which may be necessary for biological stabilization, as small trehalose molecules may be necessary for efficient hydrogen bond replacement (Carrigy & Vehring, 2019).

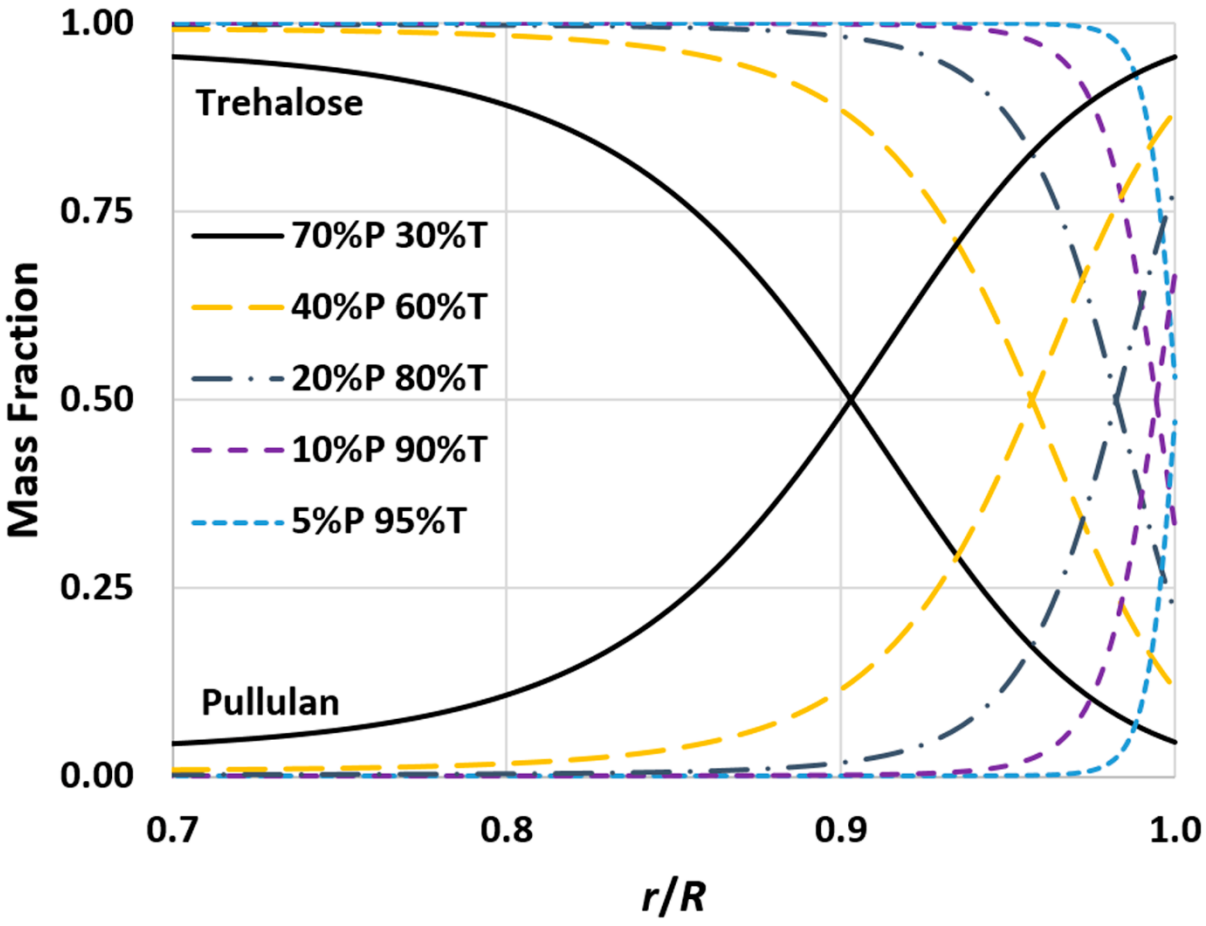

Figure 3. Internal radial distributions of mass fractions of pullulan and trehalose, demonstrating that pullulan tends to concentrate near the surface of the microparticles even at low initial mass fractions. The radial position within the microparticle, *r*, is normalized by the radius at the surface of the microparticle, *R*, on the x-axis. The legend depicts the total mass percentage of pullulan (P) and trehalose (T) in the powder. The values are approximately constant below an *r*/*R* ratio of 0.7. Colour version available online.

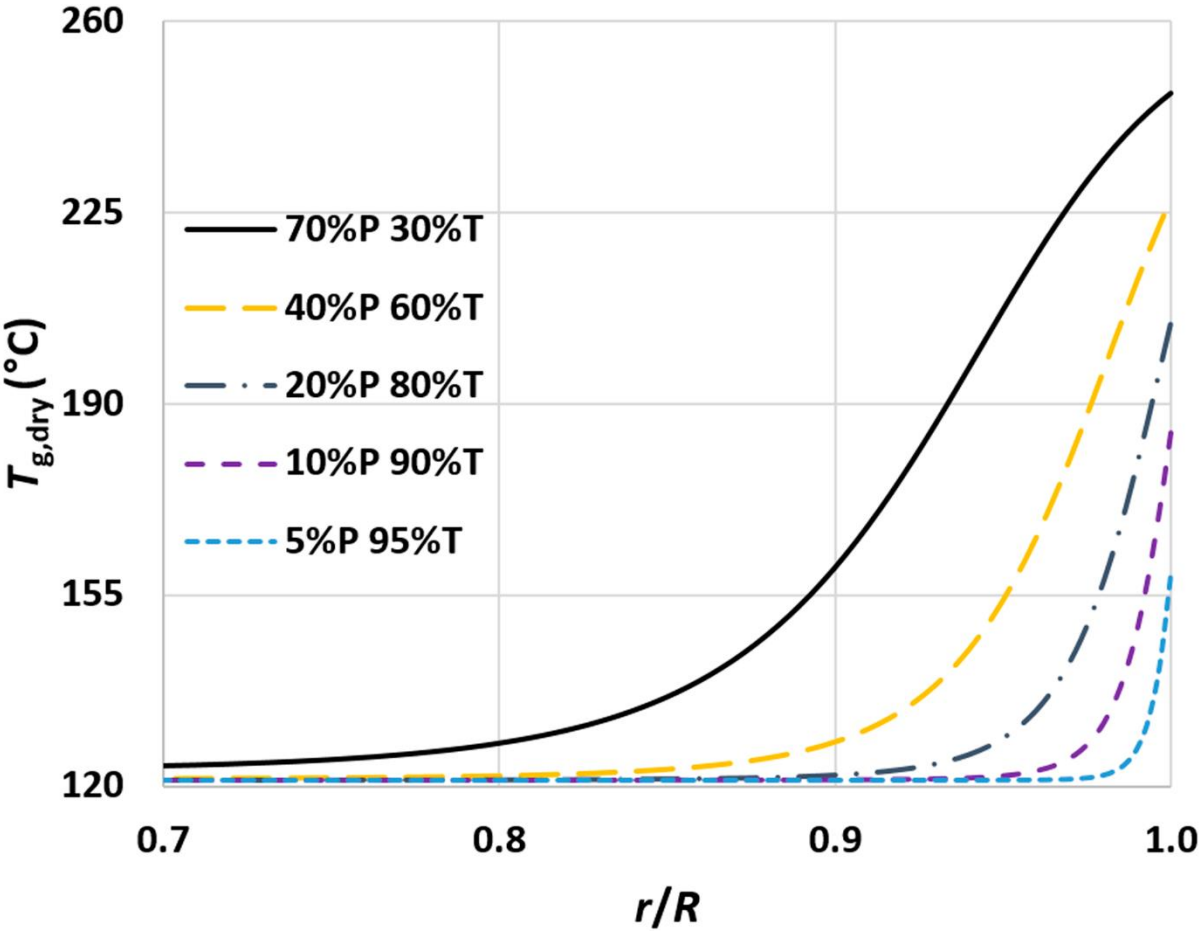

Figure 4. Internal radial distributions of local dry glass transition temperature, $T_{g,dry}$, calculated according to equation (7) using the mass fraction profiles in Figure 3. Biologics are expected to reside near the surface, where the glass transition temperature is higher, potentially leading to improved stability. The values are approximately constant below an *r*/*R* ratio of 0.7. Colour version available online.

3.2 Spray Drying

3.2.1 Spray Drying Process Model

For spray drying experiments, the droplet lifetime for a droplet emitted from the twin-fluid atomizer that is of the initial mass median diameter was 10.2 milliseconds. The

corresponding Péclet numbers for pullulan and trehalose were 21 and 1.2, respectively. This corresponded to respective steady state surface enrichments of 7.3 and 1.3.

The outlet temperature for spray drying experiments matched the predictions from the process model within 2°C. The yield was 50-65% for each case, except for the 100% pullulan content case, for which 20-25% yield was obtained and stringy particles were present (images not shown), likely due to the high viscosity of pullulan preventing droplet breakup and causing drying of jets produced during the atomization process (di Stefano, 2017). The yield, for the 0-40% pullulan content cases, is reasonable for a laboratory-scale spray dryer, demonstrating suitable manufacturability. The yield is likely to increase for larger batch sizes or for scaled-up spray dryers.

3.2.2 Spray Dried Particle Morphology

Scanning electron microscope images of the particles produced by the spray dryer are given in Figure 5. As expected for production using a twin-fluid atomizer, the microparticles are polydisperse. The trend of increasing pullulan content causing an increase in folding is in agreement with droplet chain experiments.

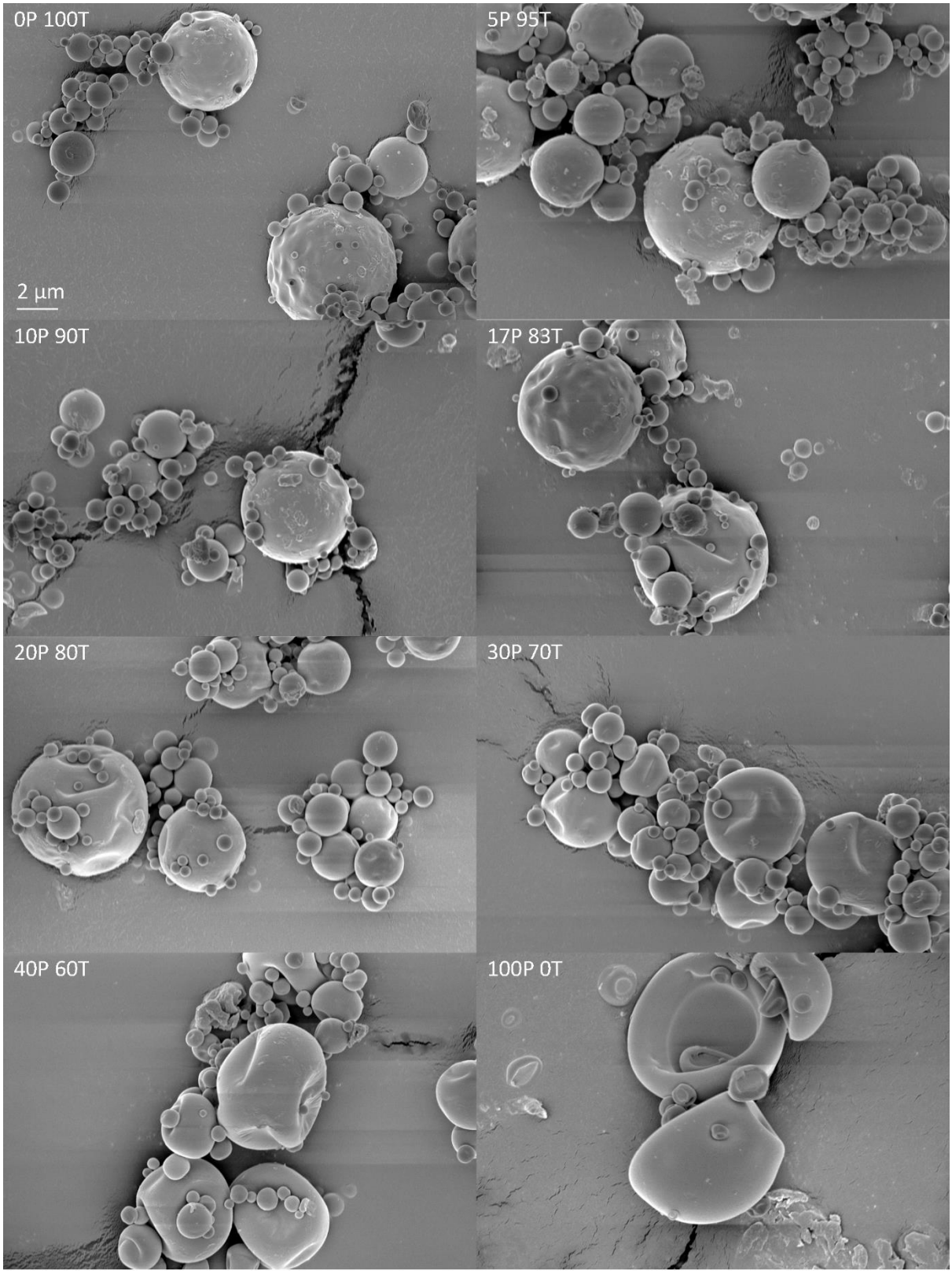

Figure 5. Scanning electron microscope images of freshly spray dried pullulan trehalose microparticles. More folding is observed for particles with a higher mass fraction of pullulan.

The microparticles are not fused. The same imaging settings were used as in Figure 1. The same scale bar applies to all images.

Helium ion microscope images of spray dried 40% pullulan 60% trehalose particles are given in Figure 6. No internal void space was detected. The theoretical particle formation models predict that water is still present in the interior when solidification is initiated at the surface. Were water in the interior of the microparticle to simply evaporate and exit as vapour diffusion through a rigid shell, interior void space would be present. The lack of interior void space in the microparticles indicates that the particles continue to shrink after solidification at the surface occurs. In reality, there is a continuous transition from dilute aqueous solution to highly viscous liquid to amorphous 'solid', and shell deformation may be occurring throughout the process, which is not currently amenable to theoretical particle formation modelling.

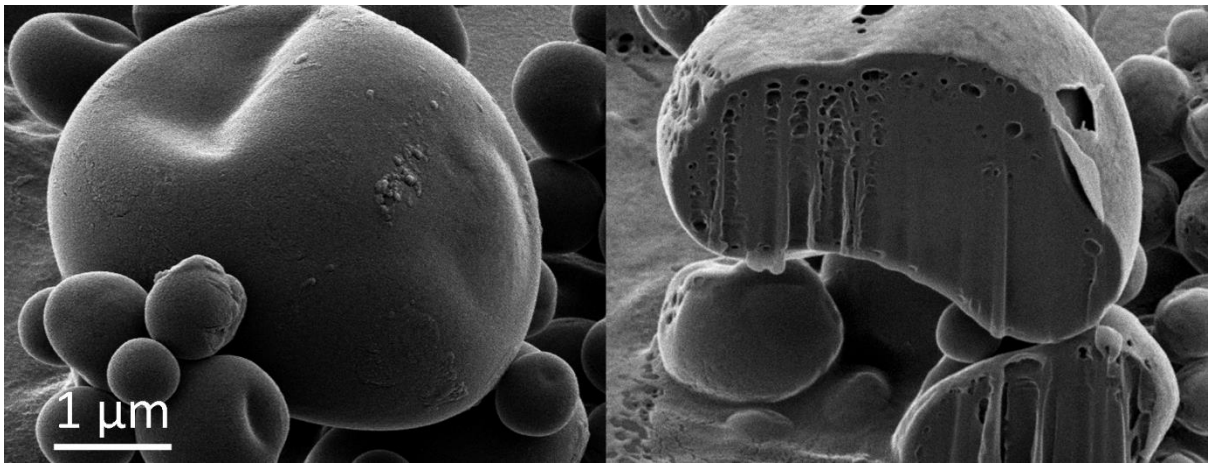

Figure 6. Helium ion microscope images of a 40% pullulan 60% trehalose microparticle before and after gallium ion beam milling. No internal void space was detected, suggesting that the particles continue to shrink after the shell is formed. The small holes visible in the cut particle on the right are artefacts of the cutting process. The peeled outer layer is the gold coating.

3.2.3 Modulated Differential Scanning Calorimetry Measurements

The results of modulated differential scanning calorimetry measurements on spray dried powders are given in Figure 7. The onset of glass transition for spray dried trehalose was near the glass transition temperature value of 121°C given by Teekamp *et al.* (2017). For spray dried pullulan, the onset of glass transition was ~255°C, slightly lower than the value of 261°C given by Teekamp *et al.* (2017). There was a glass transition at around 125°C for the spray dried pullulan trehalose powder, which is higher than the value measured for trehalose alone. This provides evidence that the pullulan addition increased the glass transition temperature relative to trehalose alone. Additionally, for pullulan trehalose powder the glass transition extended over a larger range of temperatures than for trehalose powder. The fact that the glass transition temperature occurred over a larger range of temperatures is likely due to the fact that trehalose and pullulan form a mixture with radially changing composition ratio, which was previously predicted theoretically (see Figure 4). The onset of the glass transition at 125°C for the spray dried pullulan trehalose powder likely represents the interior ($r/R < 0.7$) of the particles while the extension at higher temperatures represents the higher glass transition occurring near the surface of the particles. By adding the reversing heat flow curves of pullulan and trehalose that were spray dried individually and subtracting away the reversing heat flow curve of pullulan and trehalose spray dried together, it is evident that the spray dried pullulan trehalose has less reversing heat flow at the lower temperature and more reversing heat flow at slightly higher temperature, providing further evidence for this explanation. Furthermore, in Figure 8, the predictions for the radial profile of glass transition temperature for this powder are given. The measured glass transition range in Figure 7 for pullulan trehalose particles is within the

predicted range of 123°C at the interior to 164°C at the surface predicted by use of the numerical model and equation (7). The Fox and Gordon-Taylor equations over-predict the major component of the glass transition temperature, since they assume even mixing, i.e., constant radial profiles of mass fractions throughout the particles. In reality, the pullulan is only substantially increasing the glass transition temperature relative to trehalose near the surface, while the bulk of the powder is in the interior and is relatively unaffected and exhibits a lower glass transition temperature and earlier onset of glass transition.

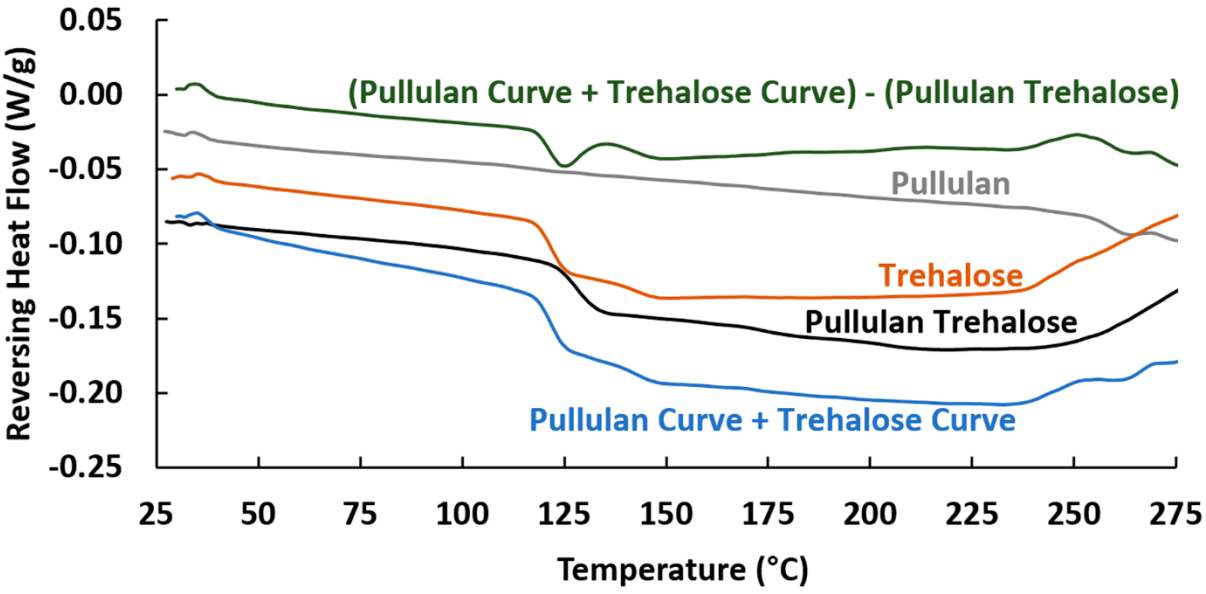

Figure 7. Modulated differential scanning calorimetry results of reversing heat flow. Spray dried pullulan trehalose powder has a higher glass transition temperature, extending over a larger range of temperatures, than trehalose alone. See the text for interpretation. "Pullulan" represents spray dried pullulan alone, "Trehalose" represents spray dried trehalose alone, "Pullulan Trehalose" represents spray dried pullulan trehalose formulation, "Pullulan Curve + Trehalose Curve" represents addition of "Pullulan" and "Trehalose" results, and "(Pullulan Curve + Trehalose Curve) - Pullulan Trehalose" represents subtraction

of “Pullulan Trehalose” from “Pullulan Curve + Trehalose Curve”. Colour version available online.

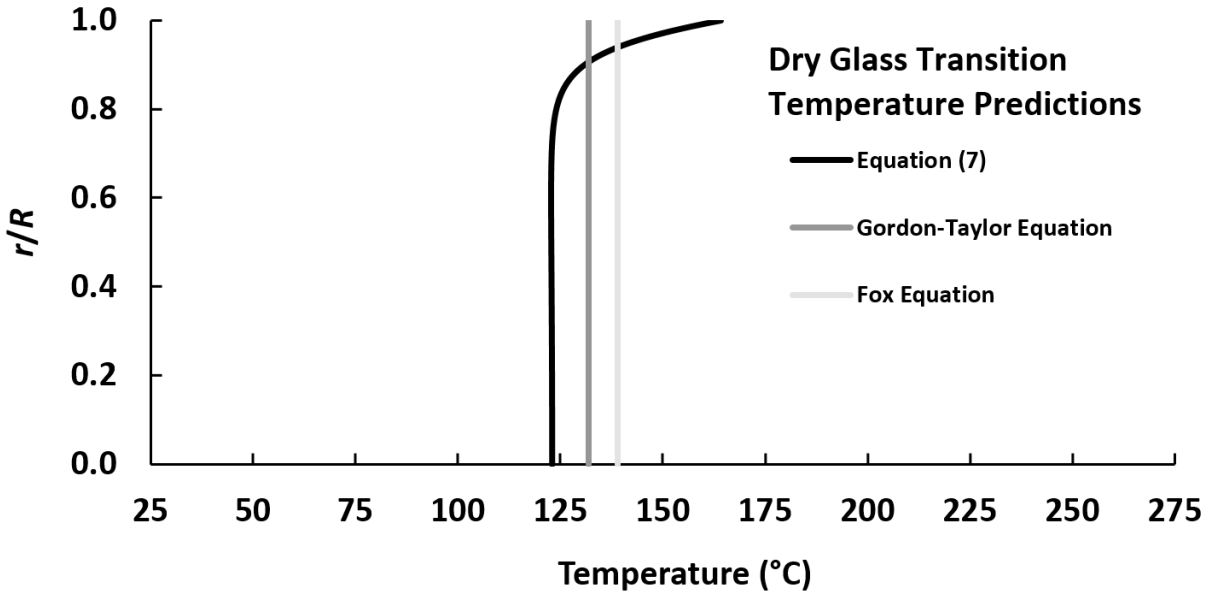

Figure 8. Radial glass transition temperature profile of 16.7% pullulan 83.3% trehalose powder predicted by use of the numerical model and equation (7) (ranging from 123°C at the interior to 164°C at the surface), as well as predictions made using the Gordon-Taylor equation (132°C) and the Fox equation (139°C), which do not vary with radius. The radial prediction is most representative of the experimental results given in Figure 7. Note that the x-axis is the same as in Figure 7 for comparison.

This is the first time, to the authors’ knowledge, that a radial profile of glass transition temperature has been predicted and experimentally supported for dry particles. As the glass transition temperature is likely to be higher near the surface due to the higher surface enrichment of pullulan as compared to trehalose, and the biologics are likely to reside near the surface, it is possible that the biologic may be glass stabilized to withstand higher temperatures or moisture contents with pullulan addition. The further effect of moisture on glass transition temperature for pullulan trehalose powder has been studied elsewhere

(Teekamp et al., 2017). Fusing between particles may be decreased under higher temperature and humidity conditions by the increased glass transition temperature at the surface. The relatively high glass transition temperature of pullulan is an advantage compared to trileucine, another amorphous excipient that concentrates at the surface and forms folded particles. Trileucine has a lower glass transition temperature, ~104°C (Lechuga-Ballesteros et al., 2008).

3.2.4 Modulated Compressed Bulk Density Measurements

The average compressed bulk density at the transition pressure was 410-470 kg/m^3 for all powders. At the transition pressure, 24-30% of the powder volume consisted of solid powder material, a reasonably high value relative to random close packing of spheres, indicating the powder is not extremely cohesive. The pullulan content, within the range of 0-40%, was not found to affect the compressed bulk density of the powders. The average transition pressure was in the range of 67-82 kPa for all powders. The powder was compressed by a factor of 1.7 ± 0.1 at this pressure, relative to the loose powder filled into the cavity. This is an important consideration for automated capsule or blister filling, e.g. when the biological dose per actuation needs to be optimized.

3.2.5 Dry Powder Inhaler Aerosol Performance Measurements

The mass collected on the different stages of the Next Generation Impactor are depicted in Figure 9. It is evident that similar aerosol performance occurred for all tested cases. The powder was easily filled into the capsules, demonstrating that the powder was flowable. For each powder the average emitted dose was 93-94% of the packaged (capsule) dose, which is promising for dry powder inhaler applications.

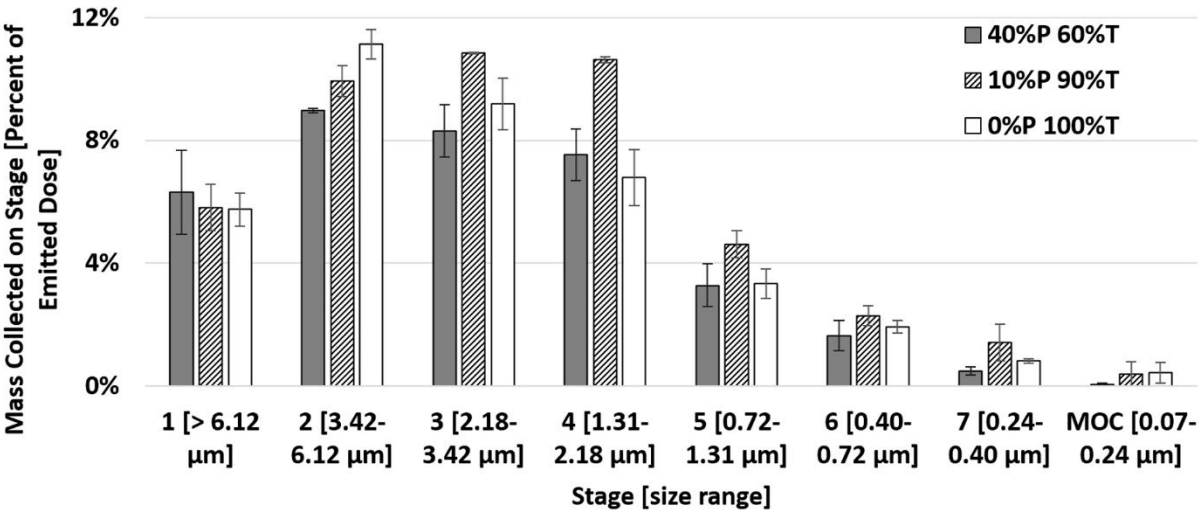

Figure 9. Mass collected past the Alberta Idealized Throat on each stage of the Next Generation Impactor for the different tested powders as a percent of the emitted dose from the Seebri® Breezhaler® dry powder inhaler. Similar trends are observed in the different cases. The error bars represent the standard deviations from two replicate measurements.

The aerosol performance results are summarized in Table 1. The total lung dose was not significantly different between any powder compositions ($p > 0.10$), although the FPF (< 6.12 µm) was significantly greater for the 10% pullulan 90% trehalose case than for the 0% pullulan 100% trehalose case ($p < 0.05$). The MMAD was not significantly different between any cases ($p > 0.05$).

Table 1. Aerosol performance of pullulan trehalose powder emitted from a Seebri® Breezhaler® dry powder inhaler through an Alberta Idealized Throat to a Next Generation Impactor.

Powder Composition	Total Lung Dose (%)	FPF (%)	MMAD (µm)

0% Pullulan 100% Trehalose	39.3 ± 1.6	30.2 ± 2.8	2.45 ± 0.03
10% Pullulan 90% Trehalose	45.9 ± 3.2	40.1 ± 2.4	2.16 ± 0.09
40% Pullulan 60% Trehalose	36.5 ± 1.4	33.6 ± 2.1	2.38 ± 0.09

Matinkhoo *et al.* (2011) summarized the total lung dose of commercially available dry powder inhalers, which ranged from 5.5-40.5%, with a mean of 23%. In the present study, pullulan trehalose microparticles had a total lung dose of 37-46%, with a mean of 41%, indicating an improvement over commercial dry powder inhalers. Therefore, spray dried pullulan trehalose powder has suitable aerosol performance for an inhalation product. Nevertheless, improvements in aerosol performance could potentially be made with additions of a dispersibility-enhancing excipient, like leucine (Feng et al., 2011; Matinkhoo et al., 2011) or trileucine (Lechuga-Ballesteros et al., 2008), although the effects of those excipients on glass stabilization and biological stability would need to be considered. From the analytical model described in Section 2.1.3 and the spray drying process model conditions in Section 2.2.1, a median particle size of 2.3-2.7 μm was predicted for these powders. The close match to the MMAD results in Table 1 supports the accuracy of the analytical model and the process model. The measured MMADs are suitable for deposition in all regions of the lung (Finlay, 2001). In each case, the GSD was ~1.9. A greater proportion of the total lung dose consisted of fine particles for increasing pullulan contents.

3.2.6 Pressurized Metered-Dose Inhaler Physical Stability Measurements

By visually examining settling of the spray dried pullulan trehalose powder within glass pressurized metered-dose inhaler canisters, it appeared that the powder maintains adequate suspension stability in either propellant after sonication for at least a few hours. The scanning electron microscope images of the powder that was kept filled in the pressurized metered-dose inhaler canisters with commercial propellants HFA 134a and HFA 227 for 42 days at 40°C, and then actuated onto a stub, are shown in Figure 10. The scanning electron microscope images indicate a similar morphology and particle size to the images of the freshly spray dried 40% pullulan 60% trehalose powder given in Figure 5. In some images, not shown, there was evidence that some particles fused, which was perhaps related to moisture ingress into the canisters, as the seal is not perfect, and the canisters were not kept in a dry box. Further improvements could potentially be made to canister sealing or with the addition of additional excipients to prevent fusing, prior to measuring the emitted particle size. Nevertheless, Raman spectra, shown in Figure 11, demonstrated that all powders remained in a completely amorphous solid phase after being kept in suspension in the different propellants for 42 days at 40°C, and subsequent actuation. The microparticles also remained amorphous after 42 days storage in a dry box, without insertion into propellant, at ambient temperature conditions. The results indicate that spray dried pullulan trehalose microparticles have promising short-term physical stability in commercial propellants even at elevated temperatures and that actuation from a pressurized metered-dose inhaler does not damage them.

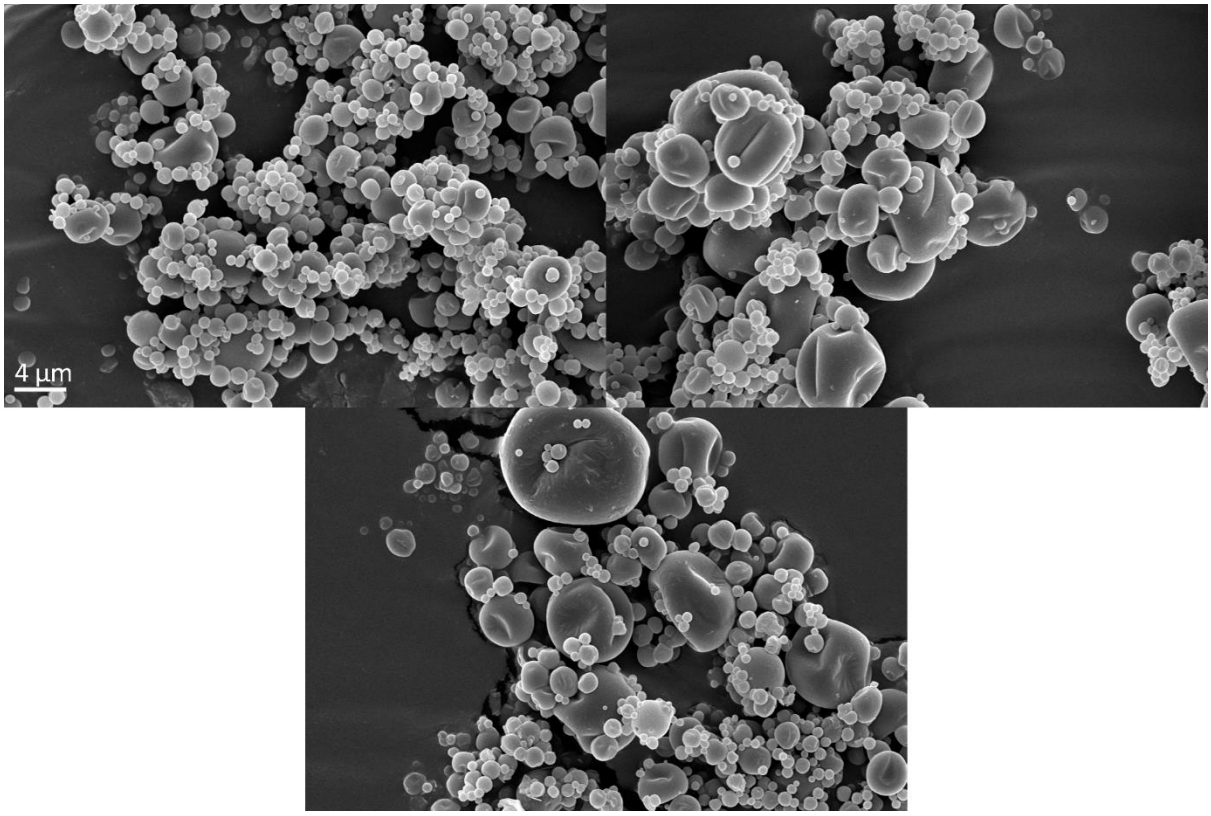

Figure 10. Scanning electron microscope images of spray dried 40% pullulan 60% trehalose microparticles after stability testing in different propellants and then actuation onto a stub via a low-flow-rate impactor. The particle morphology is similar to the freshly spray dried 40% pullulan 60% trehalose particles shown in Figure 5. Top-left: after storage and actuation from a glass canister filled with HFA 134a propellant kept at room temperature, ~22°C, for 42 days. Top-right: after storage and actuation from an aluminium canister filled with HFA 134a propellant kept at 40°C for 42 days. Bottom: after storage and actuation from a glass canister filled with HFA 227 propellant kept at 40°C for 42 days.

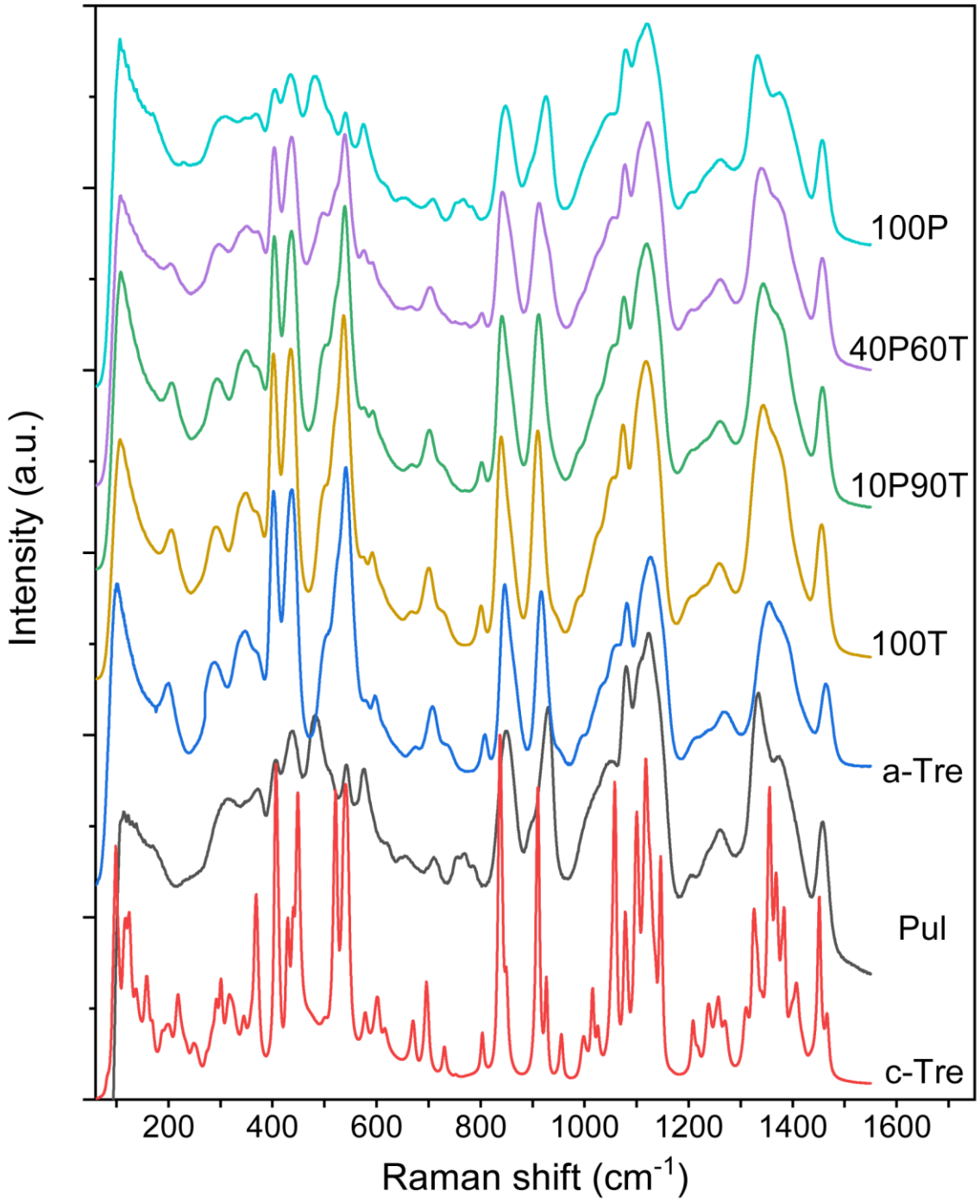

Figure 11. Raman spectra of pullulan trehalose microparticles and references, demonstrating the spray dried and stored microparticles remained in an amorphous solid phase for the different tested conditions. Legend: "c-Tre" is raw crystalline trehalose material, "Pul" is raw amorphous pullulan material, "a-Tre" is a spray dried trehalose reference from the literature (Wang et al., 2019), "100T" is spray dried 100% trehalose,

"10P90T" is spray dried 10% pullulan 90% trehalose, "40P60T" is spray dried 40% pullulan 60% trehalose, "100P" is spray dried 100% pullulan. Prior to performing Raman spectroscopy, the spray dried powder was stored for 42 days in a dry box at ambient temperature. Storage for 42 days at ambient temperature or at 40°C in commercial propellants HFA 134a and HFA 227 resulted in the same spectra as the spray dried 40% pullulan 60% trehalose powder, indicating short-term elevated temperature storage in propellant did not affect solid phase. Colour version available online.

4 Conclusions

Spray dried pullulan trehalose microparticles are a promising non-reducing sugar-only, fully amorphous platform for respiratory delivery. The suitability is justified based on measurements demonstrating acceptable manufacturability, physical stability, device compatibility, and aerosol performance.

Good manufacturability is demonstrated by a reasonable spray drying yield and the ability to easily fill the flowable powder into dry powder inhaler capsules. The manufacturability is robust, i.e., it varies little with the ratio of pullulan and trehalose in the formulation, despite increased pullulan content leading to more folded microparticles without internal void space. The powder is not too cohesive for use in inhalation devices. It can be compressed for automated filling without semi-elastic deformation. The efficient packing makes it a promising candidate for devices with small dosing volumes.

Short-term physical stability is evident as the powder maintains its amorphous phase during ambient temperature storage in a dry box and 40°C storage in pressurized metered-dose inhaler canisters containing commercial propellants HFA 134a and HFA 227. Actuation from a pressurized metered-dose inhaler does not affect the morphology or solid phase. The

powder is theoretically predicted and experimentally supported to have a higher glass transition temperature near the surface, where biologics are expected to reside, than in the interior. The higher the mass fraction of pullulan in the formulation, the more pullulan surface enrichment that occurs, and the higher the glass transition temperature at the surface, potentially resulting in more protection against fusing for temporary temperature or humidity excursions. These findings indicate that this platform likely has outstanding environmental robustness and can withstand storage at elevated temperatures. Therefore, long-term stability and environmental robustness should be assessed in future studies. Cytotoxicity of pullulan trehalose powder in the lungs should also be assessed in future studies.

The platform appears to be compatible both with dry powder inhalers and pressurized metered-dose inhalers. It has suitable aerosol performance in a commercial dry powder inhaler, exceeding that of many available commercial products. The inhalable powder is in the correct size for deposition throughout the lungs. Accurate predictions of particle diameter can be made using the newly developed particle formation model for amorphous co-solidification from multi-component drying droplets, as demonstrated by a close match of diameter predictions to experimental measurements performed using a monodisperse droplet chain. Thus, the particle formation mechanism for this type of fully amorphous particle is well enough understood so that particle formation, solid phase, and process models can be used to accelerate the development process. Further improvements to aerosol performance could potentially be made with incorporation of additional dispersibility-enhancing excipients, although it needs to be determined whether this reduces the stabilization potential of the platform.

Acknowledgements

NC thanks the Killam Trusts for providing an Izaak Walton Killam Memorial Scholarship and the University of Alberta for providing a Queen Elizabeth II Graduate Student Scholarship.

Funding

This research did not receive any specific grant from funding agencies in the public, commercial, or not-for-profit sectors.

Appendix

Previous amorphous particle formation models were limited to single-component systems. In this Appendix the time at which multicomponent amorphous systems reach the true density of the mixture at the surface of an evaporating micro-droplet and co-solidify is derived.

The total initial concentration of a mixture of dissolved solutes, $C_{0,\mathrm{mix}}$, commonly referred to as total solids content, is given by,

$$C_{0,\mathrm{mix}} = \sum_{\mathrm{i}} C_{0,\mathrm{i}} \tag{A.1}$$

where $C_{0,\mathrm{i}}$ is the initial solute concentration of solute i.

By mass conservation the total mean concentration of dissolved solutes in an evaporating droplet, $C_{\mathrm{m,mix}}$, is given by,

$$C_{\mathrm{m,mix}} = \frac{d_0^3}{d^3} C_{0,\mathrm{mix}} \tag{A.2}$$

where d is the instantaneous droplet diameter and d_0 is the initial droplet diameter.

The surface enrichment of solute i, E_{i}, is defined as,

$$E_{\mathrm{i}} = \frac{C_{\mathrm{s,i}}}{C_{\mathrm{m,i}}} \tag{A.3}$$

where $C_{\mathrm{s,i}}$ is the surface concentration of solute i and $C_{\mathrm{m,i}}$ is the mean concentration of solute i in the droplet.

The total concentration of a mixture of dissolved solutes at the surface of an evaporating droplet, $C_{\mathrm{s,mix}}$, neglecting interactions between the solutes, is given by,

$$C_{\mathrm{s,mix}} = \sum_{\mathrm{i}} C_{\mathrm{s,i}} = \sum_{\mathrm{i}} E_{\mathrm{i}} C_{\mathrm{m,i}} \tag{A.4}$$

The true density of a mixture of solids, $\rho_{\mathrm{T,mix}}$, is given by,

$$\rho_{\mathrm{T,mix}} = \frac{1}{\sum_{\mathrm{i}} \frac{Y_{\mathrm{i}}}{\rho_{\mathrm{T,i}}}} \tag{A.5}$$

where Y_{i} is the total mass fraction of solute i and $\rho_{\mathrm{T,i}}$ is the true density of solute i.

Similarly, at the surface the true density of a mixture of solids, $\rho_{\mathrm{T,mix,s}}$, is given by,

$$\rho_{\mathrm{T,mix,s}} = \frac{1}{\sum_{\mathrm{i}} \frac{Y_{\mathrm{i,s}}}{\rho_{\mathrm{T,i}}}} \tag{A.6}$$

where $Y_{\mathrm{i,s}}$ is the mass fraction of solute i at the surface, which is defined as,

$$Y_{\mathrm{i,s}} = \frac{C_{\mathrm{s,i}}}{C_{\mathrm{s,mix}}} \tag{A.7}$$

Substitution into the previous equation gives,

$$\rho_{\mathrm{T,mix,s}} = \frac{C_{\mathrm{s,mix}}}{\sum_{\mathrm{i}} \frac{C_{\mathrm{s,i}}}{\rho_{\mathrm{T,i}}}} \tag{A.8}$$

Solidification of solutes at the surface of an evaporating droplet is assumed to occur when the surface concentration of the mixture equals the true density of the mixture, i.e., when,

$$\rho_{\mathrm{T,mix,s}} = C_{\mathrm{s,mix}} \tag{A.9}$$

Therefore solidification at the surface occurs when,

$$\sum_{\mathrm{i}} \frac{C_{\mathrm{s,i}}}{\rho_{\mathrm{T,i}}} = 1 \tag{A.10}$$

By definition,

$$E_{\mathrm{i}} P_{\mathrm{i}} = \frac{C_{\mathrm{s,i}}}{C_{\mathrm{m,i}}} \frac{C_{\mathrm{0,i}}}{\rho_{\mathrm{T,i}}} \tag{A.11}$$

where P_{i} is a non-dimensional number equal to the ratio of the initial solute concentration of solute i and true density of solute i.

Therefore by substitution into the previous equation,

$$\sum_{\mathrm{i}} E_{\mathrm{i}} P_{\mathrm{i}} \frac{C_{\mathrm{m,i}}}{C_{\mathrm{0,i}}} = 1 \tag{A.12}$$

Noting that,

$$\frac{C_{\mathrm{m,i}}}{C_{\mathrm{0,i}}} = \frac{C_{\mathrm{m,mix}}}{C_{\mathrm{0,mix}}} \tag{A.13}$$

and making use of equation (A.2), the previous equation can be written,

$$\sum_{\mathrm{i}} E_{\mathrm{i}} P_{\mathrm{i}} = \frac{C_{\mathrm{0,mix}}}{C_{\mathrm{m,mix}}} = \left(\frac{d_{\mathrm{t,mix}}}{d_0}\right)^3 \tag{A.14}$$

where d_{t} is the diameter at the time for which co-solidification of a mixture occurs at the surface of a drying droplet, as this equation is only valid at that point in time due to previous assumptions.

The d^2 law is given by,

$$d^2 = d_0^2 - \kappa t \tag{A.15}$$

where d is the diameter at time t, and κ is the evaporation rate, which is assumed to be constant. The droplet lifetime, τ_{D}, is the time at which d in equation one equals zero, and is given by,

$$\tau_D = \frac{d_0^2}{\kappa} \tag{A.16}$$

Substituting into the previous equation gives,

$$\left(\frac{d}{d_0}\right)^2 = 1 - \frac{t}{\tau_{\mathrm{D}}} \tag{A.17}$$

Raising both sides to the power of 3/2 gives,

$$\left(\frac{d}{d_0}\right)^3 = \left(1 - \frac{t}{\tau_{\mathrm{D}}}\right)^{3/2} \tag{A.18}$$

Considering the time at which true density is reached at the surface and substituting into equation (A.14) gives,

$$\sum_{\mathrm{i}} E_{\mathrm{i}} P_{\mathrm{i}} = \left(1 - \frac{t_{\mathrm{t,mix}}}{\tau_{\mathrm{D}}}\right)^{3/2} \tag{A.19}$$

where $t_{\mathrm{t,mix}}$ is the time at which co-solidification occurs at the surface of a drying droplet for a mixture of dissolved solutes.

Raising both sides to the power of 2/3 and rearranging gives,

$$t_{\mathrm{t,mix}} = \tau_{\mathrm{D}} \left[1 - \left(\sum_{\mathrm{i}} E_{\mathrm{i}} P_{\mathrm{i}}\right)^{\frac{2}{3}}\right] \tag{A.20}$$

This is similar to the single-component amorphous particle formation equation given by Vehring (2008), but with a summation of the product of E_{i} and P_{i} for the individual solutes as the base number being raised to the power of 2/3.

References

Baldelli, A., Power, R.M., Miles, R.E.H., Reid, J.P., Vehring, R., 2016. Effect of crystallization kinetics on the properties of spray dried microparticles. Aerosol Sci. Technol. 50, 693-704. https://doi.org/10.1080/02786826.2016.1177163.

Boraey, M.A., Vehring, R., 2014. Diffusion controlled formation of microparticles. J. Aerosol Sci. 67, 131-143. https://doi.org/10.1016/j.jaerosci.2013.10.002.

Carrigy, N.B., Vehring, R., 2019. Engineering stable spray dried biologic powder for inhalation, in: Hickey, A.J., da Rocha, S. (Eds.), Pharmaceutical Inhalation Aerosol Technology, 3rd edition. CRC Press, Boca Raton, pp. 291-326.

Crowe, J.H., Carpenter, J.F., Crowe, L.M., 1998. The role of vitrification in anhydrobiosis. Annu. Rev. Physiol. 60, 73-103. https://doi.org/10.1146/annurev.physiol.60.1.73.

di Stefano, F., 2017. Pullulan as release enhancer for controlled release capsular device: performance assessment and preparation methods. M.Sc. Thesis. Department of Chemistry, Materials and Chemical Engineering, Politecnico di Milano, Milan, Italy.

Ekdavi-Sever, N., de Pablo, J.J., Feick, E., von Meerwall, E., 2003. Diffusion of sucrose and alpha, alpha-trehalose in aqueous solution. J. Phys. Chem. A. 107, 936-943. https://doi.org/10.1021/jp020187b.

European Food Safety Authority, 2004. Opinion of the Scientific Panel on food additives, flavourings, processing aids and materials in contact with food (AFC) on request from the Commission related to Pullulan PI-20 for use as a new food additive. EFSA J. 85, 1-32. https://doi.org/10.2903/j.efsa.2004.85.

Evaluate Ltd., 2017. EvaluatePharma® World Preview 2017, Outlook to 2022. http://www.evaluategroup.com/public/Reports/EvaluatePharma-World-Preview-2017.aspx (accessed March 9, 2018).

Feng, A.L., Boraey, M.A., Gwin, M.A., Finlay, P.R., Kuehl, P.J., Vehring, R., 2011. Mechanistic models facilitate efficient development of leucine containing microparticles for pulmonary drug delivery. Int. J. Pharm. 409, 156-163. https://doi.org/10.1016/j.ijpharm.2011.02.049.

Finlay, W.H., 2001. The mechanics of inhaled pharmaceutical aerosol: an introduction. Academic Press, London.

Fox, T.G., 1956. Influence of diluent and copolymer composition on the glass temperature of a polymer system. Bull. Am. Phys. Soc. 1, 123-128.

Gomez, M., Ordoubadi, M., McAllister, R.A., Melhem, O., Barona, D., Gracin, S., Ajmera, A., Lechuga-Ballesteros, D., Finlay, W.H., Vehring, R., 2018. Monodisperse droplet chain technique to support development of co-solvent based inhalation products, in: Dalby, R.N., Byron, P.R., Hindle, M., Peart, J., Traini, D., Young, P.M., Farr, S.J., Suman, J.D., Watts, A. (Eds.), Respiratory Drug Delivery 2018, Vol. 2. Tuscon, pp. 563-568.

Gordon, M., Taylor, J.S., 1952. Ideal copolymers and the second-order transitions of synthetic rubbers. I. non-crystalline copolymers. J. Chem. Technol. Biotechnol. 2, 493-500. https://doi.org/10.1002/jctb.5010020901.

Grasmeijer, N., Frijlink, H.W., Hinrichs, W.L.J., 2016. Model to predict inhomogeneous protein-sugar distribution in powders prepared by spray drying. J. Aerosol Sci. 101, 22-33. https://doi.org/10.1016/j.jaerosci.2016.07.012.

Hoe, S., Ivey, J.W., Boraey, M.A., Shamsaddini-Shahrbabek, A., Javaheri, E., Matinkhoo, S., Finlay, W.H., Vehring, R., 2014. Use of a fundamental approach to spray-drying formulation design to facilitate the development of multi-component dry powder aerosols for respiratory drug delivery. Pharm. Res. 31, 449-465. https://doi.org/10.1007/s11095-013-1174-5.

Kato, T., Okamoto, T., Tokuya, T., Takahashi, A., 1982. Solution properties and chain flexibility of pullulan in aqueous solution. Biopolymers. 21, 1623-1633. https://doi.org/10.1002/bip.360210812.

Krüger, P., Ehrlein, B., Zeir, M., Greguletz, R., 2014. Inspiratory flow resistance of marketed dry powder inhaler (DPI). Eur. Respir. J. 44, 4635.

Leathers, T.D., 2003. Biotechnological production and applications of pullulan. Appl. Microbiol. Biotechnol. 62, 468-473. https://doi.org/10.1007/s00253-003-1386-4.

Lechuga-Ballesteros, D., Charan, C., Stults, C.L.M., Stevenson, C.L., Miller, D.P., Vehring, R., Tep, V., Kuo, M.C., 2008. Trileucine improves aerosol performance and stability of spray-dried powders for inhalation. J. Pharm. Sci. 97, 287-302. https://doi.org/10.1002/jps.21078.

Leung, V., Szewczyk, A., Chau, J., Hosseinidoust, Z., Groves, L., Hawsawi, H., Anany, H., Griffiths, H.W., Ali, M.M., Filipe, C.D.M., 2018. Long-term preservation of bacteriophage antimicrobials using sugar glasses. ACS Biomater. Sci. Eng. 4, 3802-2808. https://doi.org/10.1021/acsbiomaterials.7b00468.

Marple, V.A., Olson, B.A., Santhanakrishnan, K., Mitchell, J., Murray, S.C., Hudson-Curtis, B.L., 2003. Next generation pharmaceutical impactor (a new impactor for pharmaceutical inhaler testing). Part II: archival calibration. J. Aerosol Med. Pulm. Drug Deliv. 16, 301-324. https://doi.org/10.1089/089426803769017668.

Matinkhoo, S., Lynch, K.H., Dennis, J.J., Finlay, W.H., Vehring, R., 2011. Spray-dried respirable powders containing bacteriophages for the treatment of pulmonary infections. J. Pharm. Sci. 100, 5197-5205. https://doi.org/10.1002/jps.22715.

Nishinari, K., Kohyama, K., Williams, P.A., Phillips, G.O., Burchard, W., Ogino, K., 1991. Solution properties of pullulan. Macromolecules 24, 5590-5593. https://doi.org/10.1021/ma00020a017.

Ohtake, S., Wang, Y.J., 2011. Trehalose: current use and future applications. J. Pharm. Sci. 100, 2020-2053. https://doi.org/10.1002/jps.22458.

Ordoubadi, M., Gregson, F., Finlay, W.H., Vehring, R., Reid, J.P., 2018. Interaction of evaporating multicomponent microdroplets with humid environments, in: Dalby, R.N., Byron, P.R., Hindle, M., Peart, J., Traini, D., Young, P.M., Farr, S.J., Suman, J.D., Watts, A. (Eds.), Respiratory Drug Delivery 2018, Vol. 2. Tuscon, pp. 569-572.

Rekha, M.R., Sharma, C.P., 2007. Pullulan as a promising biomaterial for biomedical applications: a perspective. Trends Biomater. Artif. Organs 20, 116-121.

Ruzycki, C.A., Martin, A.R., Vehring, R., Finlay, W.H., 2018. An *in vitro* examination of the effects of altitude on dry powder inhaler performance. J. Aerosol Med. Pulm. Drug Deliv. 31, 221-236. https://doi.org/10.1089/jamp.2017.1417.

Sangon Biotech, 2018. Safety Data Sheets: Pullulan. https://www.sangon.com/productImage/SDS/A506209/A506209_EN_S.pdf (accessed January 18, 2019).

Schwartzbach, H., 2011. Achieving aseptic drying with spray drying technologies. Pharmaceutical Technology Europe 23, 90-92. http://www.pharmtech.com/achieving-aseptic-drying-spray-drying-technologies

Shahrbabak, A.S., 2013. Uniaxial compression of pharmaceutical powders. M.Sc. Thesis, Department of Mechanical Engineering, University of Alberta, Edmonton, Canada.

Siew, A., 2016. Exploring the use of aseptic spray drying in the manufacture of biopharmaceutical injectables. Pharmaceutical Technology 40, 24-27. http://www.pharmtech.com/exploring-use-aseptic-spray-drying-manufacture-biopharmaceutical-injectables.

Sugumaran, K.R., Ponnusami, V., 2017. Review of production, downstream processing and characterization of microbial pullulan. Carbohydr. Polym. 173, 573-591. https://doi.org/10.1016/j.carbpol.2017.06.022.

Teekamp, N., Tian, Y., Visser, J.C., Olinga, P., Frijlink, H.W., Woerdenbag, H.J., Hinrichs, W.L.J., 2017. Addition of pullulan to trehalose glasses improves the stability of β-galactosidase at high moisture conditions. Carbohydr. Polym. 176, 374-380. https://doi.org/10.1016/j.carbpol/2017.08.084.

Tian, Y., Visser, C.J., Klever, J.S., Woerdenbag, H.J., Frijlink, H.W., Hinrichs, W.L.J., 2018. Orodispersible films based on blends of trehalose and pullulan for protein delivery. Eur. J. Pharm. Biopharm. 133, 104-111. https://doi.org/10.1016/j.ejpb.2018.09.016.

Tsapis, N., Dufresne, E.R., Sinha, S.S., Riera, C.S., Hutchinson, J.W., Mahadevan, L. Weitz, D.A., 2005. Onset of buckling in drying droplets of colloidal suspensions. Phys. Rev. Lett. 94, 018302. https://doi.org/10.1103/PhysRevLett.94.018302.

United States Food and Drug Administration, 2019a. GRAS Notices: GRN No. 99. https://www.accessdata.fda.gov/scripts/fdcc/index.cfm?set=GrASNotices&id=99&sort=GRN_No&order=DESC&startrow=1&type=advanced&search=%C2%A4%C2%A4pullulan%C2%A4 (accessed 26 March 2019).

United States Food and Drug Administration, 2019b. GRAS Notices: GRN No. 45. https://www.accessdata.fda.gov/scripts/fdcc/index.cfm?set=GrASNotices&id=45 (accessed 26 March 2019).

United States Pharmacopeia, 2017. <601> Aerosols, nasal sprays, metered-dose inhalers, and dry powder inhalers.

Vehring, R., Foss, W.R., Lechuga-Ballesteros, D., 2007. Particle formation in spray drying. J. Aerosol Sci. 38, 728-746. https://doi.org/10.1016/j.aerosci.2007.04.005.

Vehring, R., 2008. Pharmaceutical particle engineering via spray drying. Pharm. Res. 25, 999-1022. https://doi.org/10.1007/s11095-007-9475-1.

Walsh, G., 2014. Biopharmaceutical benchmarks 2014. Nat. Biotechnol. 32, 992-1000. https://doi.org/10.1038/nbt.3040.

Walters, R.H., Bhatnagar, B., Tchessalov, S., Izutsu, K.I., Tsumoto, K., Ohtake, S., 2014. Next generation drying technologies for pharmaceutical applications. J. Pharm. Sci. 103, 2673-2695. https://doi.org/10.1002/jps.23998.

Wang, H., Boraey, M.A., Williams, L., Lechuga-Ballesteros, D., Vehring, R., 2014. Low-frequency shift dispersive Raman spectroscopy for the analysis of respirable dosage forms. Int. J. Pharm. 469, 197-205. https://doi.org/10.1016/j.ijpharm.2014.04.058.

Wang, H., Bhambri, P., Ivey, J., Vehring, R., 2017. Design and pharmaceutical applications of a low-flow-rate single-nozzle impactor. Int. J. Pharm. 533, 14-25. https://doi.org/10.1016/j.ijpharm.2017.09.047.

Wang, H., Nobes, D.S., Vehring, R., 2019. Particle surface roughness improves colloidal stability of pressurized pharmaceutical suspensions. Pharm. Res. 36, 43. https://doi.org/10.1007/s11095-019-2572-0.